MORPHOLOGICAL AND STRUCTURAL CHARACTERIZATION OF SINTERED COMPACTS ZIRCONIUM-ERBIUM OBTAINED BY POWDER METALLURGY

Nicolae Tiberiu CIOBANU[1,2,*], Adriana-Gabriela SCHIOPU[3], Daniela DIACONU[1,3], Catalin Marian DUCU[3], Mihai OPROESCU[3], Maria Magdalena DICU[3], Denis Aurelian NEGREA[4], Sorin GEORGIAN MOGA[4], Mariana POSTELNICU[1], Vasile RADU[1]

This work aims to obtain sintered zirconium-erbium alloys with different compositions using powder metallurgy. Zirconium and erbium precursor powders were prepared by separate hydriding at 750 °C, in hydrogen atmosphere at a pressure of 10^5 Pa. The resulting hydrides were ground, sieved, weighed, and mixed, then hydraulically pressed into cylindrical compacts at a pressure of $1.16*10^7$ Pa. The green compacts were sintered at 1200 °C in an inert atmosphere. After sintering, the samples were characterized in terms of density, microstructure by SEM-EDS, and phase composition by XRD. The results show that samples with higher erbium content exhibit higher density. Microstructural analysis indicates a multiphase structure consisting of zirconium-rich solid solution. XRD analysis reveals that Zr-rich compositions tend to form a larger fraction of Zr–Er phases within the $Er_{0.15}Zr_{0.85}$ alloy composition.

Keywords: powder metallurgy, sintering, hydriding, zirconium, erbium, alloys

1. Introduction

Hydrogen is a flexible energy carrier that can be produced in a variety of ways and has the potential to revolutionise the global energy landscape **[1]**. Using hydrogen as an energy solution is in line with global efforts to curb climate change and reduce greenhouse gas emissions. The use of hydrogen-based technologies can significantly reduce carbon dioxide (CO_2) emissions. According to the International Energy Agency (IEA), global hydrogen production has been growing steadily over the years **[2]**.

[1]* Scientific Researcher, Nuclear Materials, Corrosion and Surface Analysis Department, Institute for Nuclear Research, Mioveni, Romania, correspondent author, e-mail: tiberiu.ciobanu@nuclear.ro
[2] PhDs, National University of Science and Technology POLITEHNICA Bucharest, Pitesti University Centre, Doctoral School Materials Science and Engineering, Pitesti, Romania
[3] National University of Science and Technology POLITEHNICA Bucharest - Pitesti University Centre, Faculty of Mechanics and Technology, Pitesti, Romania, e-mail: gabriela.schiopu@upb.ro
[4] National University of Science and Technology POLITEHNICA Bucharest, Pitesti University Centre, Regional center of research & development for materials, processes and innovative products dedicated to the automotive industry (CRC&D-AUTO), Pitesti, Romania, e-mail: aurelian.negrea@upb.ro

Hydrogen, as an energy source, has higher energy efficiency (about 60%) compared to conventional fuels **[3]**. However, the volumetric density of gaseous hydrogen is 0.082 kg/m^3 under standard conditions, which is relatively low compared to fossil fuels **[4]**. Storing such a rarefied gas requires a large cylinder and a high compression ratio of up to 700 bar at ambient temperature. However, even at such a high compression ratio, the volumetric energy density is still low, which poses a significant challenge for its use in vehicles **[5] [6] [7]**. Furthermore, hydrogen compression is an energy-intensive process, with the energy consumption for compression to 600 bar being 20.5 MJ/kg **[8]**. Similar 100 wt% gravimetric capacities were observed for liquid hydrogen operating at −253 °C and in the 1÷10 bar pressure range. However, the biggest challenges lie in maintenance, handling, and transmission losses at cryogenic temperatures, which severely limit practical applications **[9] [10]**. To address these issues, material-based storage solutions have been developed using the interaction of hydrogen with materials. Hydrogen is able to be stored as metal hydrides, with a various applications: energy storage, heating and cooling systems etc. **[11]**.

The metal-hydrogen systems are often used as model systems to study physical or chemical properties and their change with concentration **[12]**. A material that can be used for hydrogen storage system is zirconium-erbium alloy; both have the property of absorbing/releasing hydrogen, under certain conditions.

The zirconium-hydrogen system has been studied in many papers, from which it can be concluded that zirconium stored hydrogen, under certain conditions. According to the data reported in **[13]**, zirconium interacts with hydrogen over two distinct temperature ranges. Between 200ºC and 550ºC, zirconium exists predominantly as an α-Zr solid solution, within which the maximum hydrogen solubility reaches approximately 5.9 at.%. At higher temperatures, ranging from 550ºC to 863ºC, zirconium undergoes further hydrogen absorption and bonding, being present mainly in the β-Zr phase with a hydrogen concentration of about 37.5 at%, as well as in the σ phase, characterized by an H/Zr atomic ratio between 1.6 and 1.8 **[13]**.

Erbium-hydrogen system has not been studied often in research. There are few papers about the interaction between erbium and hydrogen. According to the data reported in [14], erbium forms hydride phases with hydrogen, namely ErH_2 and ErH_3. The ErH_2 phase is stable at temperatures up to approximately 500 °C, corresponding to a hydrogen content in the range of 1–1.5 wt.%. At higher temperatures, up to about 750 °C, the ErH_3 phase is formed, with the hydrogen concentration remaining below 2 wt.% [14].

Over the years, in the research activities carried out worldwide, the binary system Er-Zr has been studied by various researchers [15-18]. According to the results reported in [18], Er–Zr alloys exhibit two principal solid solutions: an Er-rich solid solution corresponding to the low-temperature α-Er phase and a Zr-rich

solid solution associated with the high-temperature β-Zr phase. Below the eutectic temperature of approximately 1450 °C and above 925 °C, these elements coexist predominantly in the form of α-Er and β-Zr phases, depending on the specific erbium and zirconium concentrations in the alloy [18].

The main methods of manufacturing alloys can be carried out by different methods:

1. Melting method, the most common industrial method used for producing alloys [19];
2. Powder metallurgy, a process where the elements are converted into powders, mixed in precise proportions, compacted and sintered below their melting points [20];
3. Solid-State diffusion, where elements are placed in close contact and heated below their melting temperatures [21];
4. Mechanical alloying, which use high-energy ball milling to repeatedly fracture and cold-weld particles of the elements [22].

The aim of this work is to fabricate sintered Zr–Er compacts with different compositions by powder metallurgy and to investigate their morphological and structural characteristics as a function of composition. The powder metallurgy method was chosen, offering numerous advantages over other methods, such as:

- Avoidance of extremely high melting temperatures, that demand specialized furnaces and protective atmospheres due to zirconium strong affinity for oxygen and nitrogen. Powder metallurgy allows alloy formation through solid-state sintering below melting temperatures, significantly reducing thermal and equipment requirements;
- Reduced oxidation and contamination, both zirconium and erbium oxidize readily at high temperatures. PM processing is typically carried out in vacuum or inert atmospheres, minimizing oxidation and contamination compared to liquid-state processing;
- Improved composition control, powder metallurgy enables precise control of Zr–Er composition by accurately weighing and mixing elemental powders;
- Lower material loss and cost efficiency, powder metallurgy minimizes losses due to evaporation, slag formation, or oxidation, making it a more economical route for Zr–Er alloy development.

To obtain Zr-Er compacts with different compositions, through powder metallurgy, starting from raw materials of pure zirconium and erbium metals, the following steps must be followed:

1. Separate hydriding of the raw materials, in order to embrittle the initial metals and facilitate subsequent processing operations of the hydrides obtained;

2. Grinding and sieving of erbium and zirconium hydrides, in order to obtain fine powders with a certain granulation;
3. Dosing, mixing and pressing of the precursor powders, in order to obtain pressed compacts with the desired concentrations and dimensions;
4. Sintering heat treatment, at certain preset parameters, in order to obtain the desired final compacts.

2. Materials and methods

2.1. Hydriding raw materials

To obtain sintered erbium–zirconium compounds via powder metallurgy with compositions of Zr_{75}–Er_{25} and Zr_{50}–Er_{50}, zirconium and erbium powders were first prepared by separate hydriding of the constituent elements. This hydriding treatment was required to facilitate subsequent processing of the precursors, as hydrogen-induced embrittlement promotes material fragmentation and enables the production of fine powders with reduced grain size. Commercial sponge zirconium supplied by Wah Chang (Albany, USA), with a purity exceeding 99%, was hydrided in a furnace at 750 °C for 120 minutes under a dynamic hydrogen atmosphere at a pressure of 10^5 Pa. The equation that describes the interaction between Zr and H_2 is:

$$Zr + H_2 \rightarrow ZrH_2 \quad (1)$$

The same treatment was performed for metallic erbium from Hefa Rare Earth Canada, which has a purity over 99.9%, using Hydrogen 6.0 from Linde Company, Romania, at a temperature level of 120 minutes, in dynamic atmosphere, at a pressure of 10^5 Pa. Equation that describes the interaction between Er and H_2 is:

$$2Er + 3H_2 \rightarrow 2ErH_3 \quad (2)$$

2.2. Pressing samples

The obtained hydrides were weighed at the desired proportions, in order to obtain two batches of precursor mixture having the following concentrations: 50% ZrH_2 – 50%ErH_3 and 75%ZrH_2 – 25% ErH_3. Then, each precursor batch was grounded in a ceramic mortar with pestle, in order to obtain fine powders. After grinding, the mixture powders were sieved using a stainless steel sieve with a grain size of 32 μm. These two processes were repeated until all quantity of hydrides mixture has the desire grain size.

The powder mixture batches were pressed using a cylindrical stainless steel die, with diameter 15.5 mm, using a manual unilateral hydraulic press. The pressed compacts were obtained by pressing the powders at a pressure of $1.16*10^7$ Pa, which was maintained for 30 seconds. Following the pressing operation, were

obtained two green pellets: 50% ZrH_2 - 50% ErH_3 and 75% ZrH_2 – 25% ErH_3 (Fig. 1).

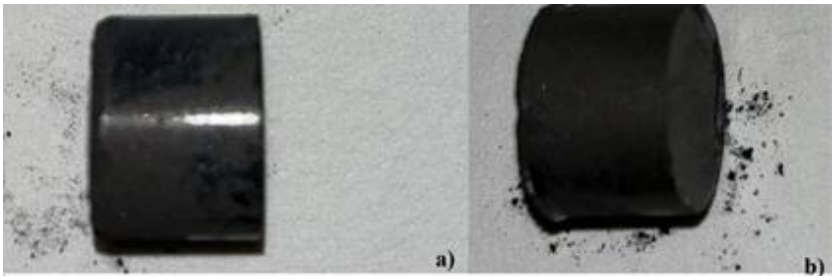

Fig. 1.a) Pressed sample 75%ZrH_2 - 25% ErH_3; b) Pressed sample 50%ZrH_2-50%ErH_3

The samples were weighed using an analytical balance, measured with a digital caliper to determine their height and diameter, the measurements being made in three different points. Using the geometric characteristics obtained, the densities of the samples were determined using the formula:

$$\rho_{sample} = \frac{m}{V}, \quad (3)$$

where m is the mass of the sample and V is the volume of the sample. Table 1 presents the geometric properties of the green compacts.

Table 1

Geometric properties of pressed samples

Sample number	Content	Geometric density (g/cm^3)
1	75%ZrH_2-25%ErH_3	4.50
2	50%ZrH_2-50%ErH_3	4.65

After pressing, the samples were subjected to the sintering thermal treatment.

2.3. Sintering treatment

The sintering treatment was performed in furnace, using a Ta resistance, in dynamic atmosphere of He 6.0, at a pressure of 10^5 Pa. The samples were placed in the furnace, after which the vacuum operation was performed, to eliminate impurities from the furnace, and finally, it was supplied with helium. The working temperature was chosen as 2/3 of the melting temperature of the material with the highest melting point ($ZrT_{melting}$ = 1852 ^oC) [23]. Also, for the selection of the working temperature, the complete dehydration of the samples is also aimed. The sintering of the compacts was performed according to the thermal diagram shown in Fig. 2.

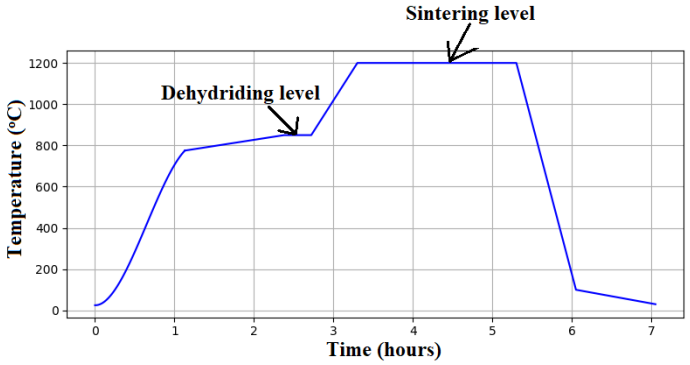

Fig. 2. Thermal diagram of sintering treatment Zr_x-Er_{1-x}

2.4. Analysis methods description

Following the hydriding of the Zr and Er raw materials, the resulting powders were examined for their structural characteristics by XRD. This analysis was performed with 'PANALYTICAL X'PERT PRO MPD' computerized diffractometer (Malvern Panalytical Ltd, Malvern, United Kingdom), equipped with proportional detector with encapsulated gas (xenon), X-ray tube with Cu anode, curved graphite monochromator for Cu Kα radiation and a vertical goniometer.

The morphology of Zr_xEr_{1-x} (x = 0.50; 0.75), were examined using Tescan VEGA II LMU scanning electron microscope (TESCAN GROUP, Brno – Kohoutovice, Czech Republic) under vacuum conditions.

The densities of the samples were experimentally determined via immersion in demineralized water at room temperature and atmospheric pressure, using RADWAG XA 160/X analytical balance (RADWAG, Poland).

Morphologycal analysis of the sintering samples were conducted with HITACHI SU5000 scanning electron microscope, which is equipped with an energy-dispersive X-ray spectroscopy (EDS) module (Hitachi, Tokyo, Japan) for elemental composition analysis.

The structural characterization of sintered compounds were performed using Rigaku Ultima IV X-ray diffractometer (Rigaku Corporation, Tokyo, Japan), equipped with a D/teX Ultra detector, graphite monochromator for Kβ radiation and a vertical goniometer, in Bragg-Brentano focusing.

3. Results and discussion

3.1. Precursors characterization

Structural analysis of hydrides was performed to determine the phases formed following hydriding treatment of raw materials, and to determine the crystal structures of the phases and the concentrations of them. XRD analyses of the samples were performed at room temperature. Each erbium hydride and zirconium hydride powder was analyzed separately.

According to the analyses, it was found that the main phase found is ErH_3 phase, in a concentration of 98 wt.%, formed following the hydriding treatment of pure metallic erbium. Also, small amounts of 2 wt.% impurities in the form of the $ErO_{1.5}$ phase were found. The phase concentrations were determined by the Reference Intensity Ratio (RIR) Method. Table 2 presents the crystallographic properties of the compounds found. All phases existing in the sample were identified using the ICDD PDF4+ database, provided by ICDD USA.

Table 2

Crystallographic properties of erbium hydride powder

Phase	Crystal structure	Lattice parameters		
		a (Å)	b (Å)	c (Å)
ErH_3	hexagonal	3.621	3.621	6.525
$ErO_{1,5}$	cubic	5.165	5.165	5.165

From XRD analysis of zirconium hydride, the following phases were found: ZrH_2, in a concentration of 72 wt.% and pure zirconium, in a percentage of 28 wt.%. All present phases were identified using the ICDD PDF4+ database, provided by ICDD USA. Table 3 presents the crystallographic properties of the phases found.

Table 3

Crystallographic properties of zirconium hydride powder

Phase	Crystal structure	Lattice parameters		
		a(Å)	b(Å)	c(Å)
ZrH_2	Tetragonal	3.51	3.51	4.46
Zr	Hexagonal	3.249	3.249	5.203

3.2. Geometric characterization

The geometric characterization of the sintered $Zr_x - Er_{1-x}$ samples, where x is 0.50 and 0.75, was performed by determining their mass, using an analytical balance, after that the samples were measured in height and diameter, in three different points. The density of the samples was determined by immersion, using RADWAG XA 160/X analytical balance, in demineralized water at room temperature and atmospheric pressure. In order to be able to compare the experimental results obtained, the theoretical density of the samples was determined using the following formula:

$$\rho_{ZrxEr1-x} = \rho_{Zr} * x + \rho_{Er} * (1-x), \quad (3)$$

where ρ_{Zr} is the density of zirconium, ρ_{Er} is the density of erbium, and x has the value: 0.50 and 0.75; depending on the sample analyzed. Table 4 presents the geometric characteristics obtained for each sample.

Table 4

Geometric properties of sintered compacts

Sample number	Content	Geometric density (g/cm^3)	Experimental density (g/cm^3)	Theoretical density (g/cm^3)
1	$Zr_{75}Er_{25}$	5.94	6.7102	7.1675

2	$Zr_{50}Er_{50}$	7.24	7.3670	7.845

3.3. Morphological analysis

The morphological analysis of the sintered compounds was performed using TESCAN VEGA II LMU electronic microscope. In order to analyze the samples, they were prepared by cutting small samples and grinding them. The grinding process was performed using BUEHLER GRINDER-POLISHER BETA 2, at a speed of 250 rpm. Fig. 3 presents the micrographs of $Zr_{75}Er_{25}$ sample.

Fig. 3.a) the sample $Zr_{75}Er_{25}$ is analyzed microscopically, using a BSE detector, at 500X. The elements zirconium and erbium are well contrasted, zirconium being associated with the dark gray color, and erbium being associated with the light gray color, these associations being made by the atomic number of each element. To porosity of the sample is identified as the black areas from the Fig. 3.a).

In Fig. 3.b) it can be observed that the elements interact during the sintering treatment, resulting in a mechanical mixture of phases [24].

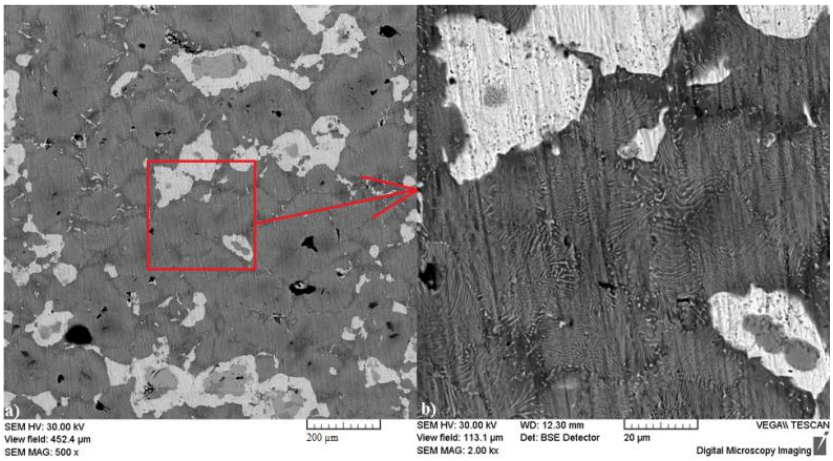

Fig. 3. SEM analysis of $Zr_{75}Er_{25}$ a) 500X, BSE detector; b) 2000X, BSE detector

Fig. 4 presents the micrographs obtained by analyzing the sintered sample $Zr_{50}Er_{50}$. Micrograph 4.a) shows the surface of analyzed $Zr_{50}Er_{50}$ sample, using BSE detector, at 500X magnification. The particles of the sample can be distinguished, zirconium being associated with the dark gray color, and erbium is associated with the light gray color. A homogeneous distribution of the two elements can be observed. In Fig. 4.b), the sample corresponding to the region highlighted in Fig. 4.a) is examined using a backscattered electron (BSE) detector at a magnification of 2000X. Under these imaging conditions, the two constituent elements are more clearly distinguished, confirming the formation of a solid solution between erbium and zirconium. After sintering, the alloy presents a mechanical mixture of phases due to incomplete diffusion of erbium into the

zirconium matrix. According to the zirconium–erbium phase diagram reported in Ref. [18], at a temperature of 1200 °C and for the investigated erbium and zirconium compositions, the system consists of the α-Er and β-Zr phases.

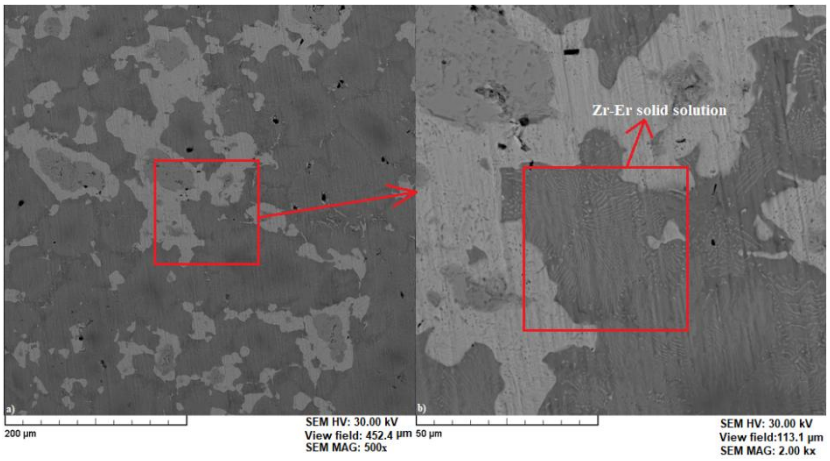

Fig. 4. SEM analysis of $Zr_{50}Er_{50}$ a) 500X, BSE detector; b) 2000X, BSE detector

To investigate the elemental distribution in the $Zr_{75}Er_{25}$ sample after heat treatment, a representative region at the interface between the constituent elements was selected and analyzed by SEM–EDS at a magnification of 2000X (Fig. 5). This analysis was performed to evaluate the interaction between zirconium and erbium during the sintering process. The SEM–EDS elemental mapping results presented in Fig. 5 show regions where zirconium and erbium coexist, suggesting significant interdiffusion between the two elements. This behavior is attributed to the diffusion of erbium into Zr-rich regions during the sintering heat treatment, promoted by enhanced atomic mobility at elevated temperatures. Furthermore, the oxygen distribution highlights a higher oxygen concentration in erbium-rich regions, confirming the pronounced affinity of erbium for oxygen and its tendency to form oxide phases.

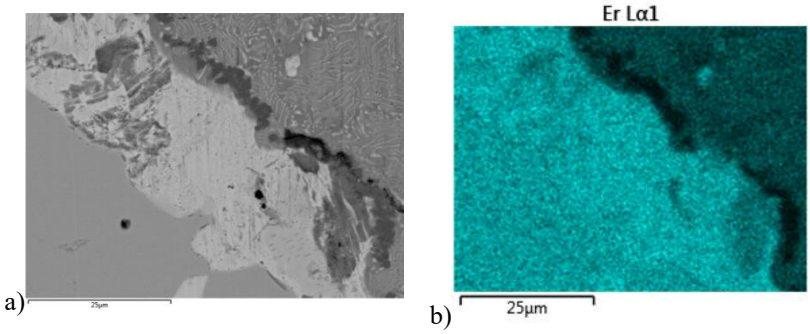

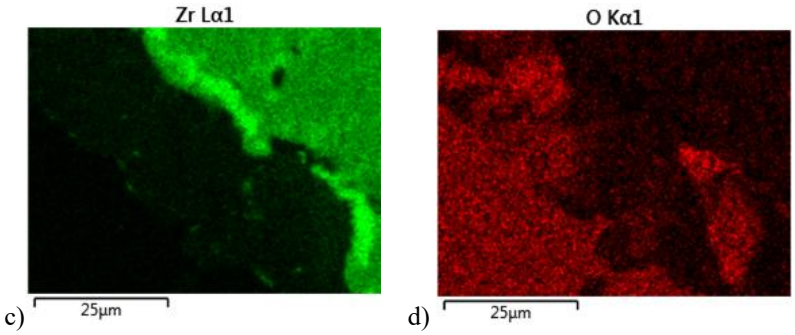

Fig. 5.a) SEM micrograph of $Zr_{75}Er_{25}$, 2000X, BSE detector; b)-d) Er, Zr and O elemental distribution

To perform a qualitative elemental analysis aimed at assessing the interaction between zirconium and erbium, the $Zr_{50}Er_{50}$ sample was characterized by SEM–EDS at a magnification of 3000X (Fig. 6).

The elemental analysis of the $Zr_{50}Er_{50}$ sample reveals the simultaneous presence and spatial overlap of zirconium and erbium, indicating significant interdiffusion at the microscale between the two elements. This behavior is attributed to the diffusion of erbium into the zirconium matrix during the heat treatment, which promotes atomic bonding and the formation of Er–Zr solid solution phases. Additionally, higher oxygen concentrations are observed in erbium-rich regions, confirming the strong affinity of erbium for oxygen and its pronounced tendency to form oxide phases.

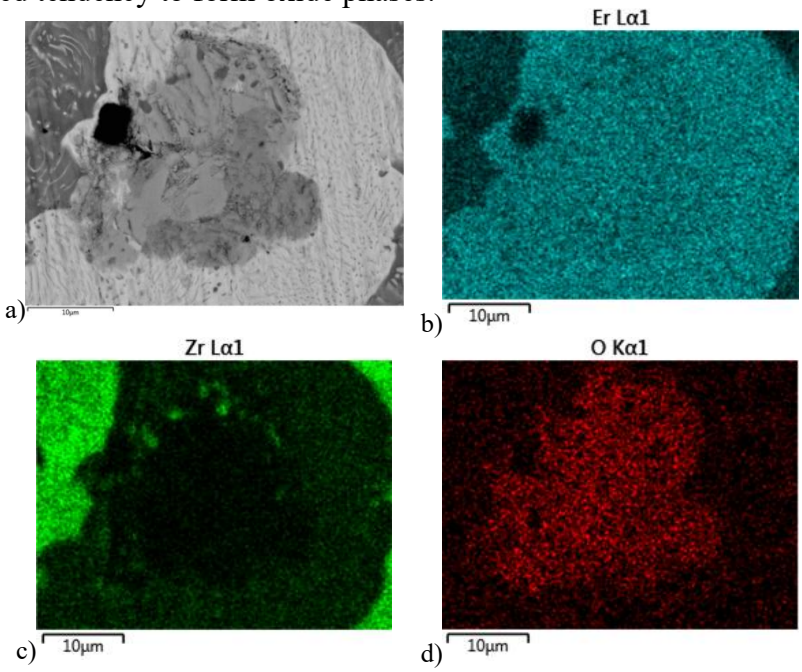

Fig. 6. a) SEM micrograph of $Zr_{50}Er_{50}$, 3000X, BSE detector; b)-d) Er, Zr and O elemental distribution

3.4. Structural analysis

The XRD structural analysis of $Zr_{75}Er_{25}$ sample was performed using the Rigaku Ultima IV X-ray diffractometer.

The diffractogram of $Zr_{75}Er_{25}$ was obtained using CuKα radiation in the measurement range 2θ: (25°-105°), by continuous scanning, with a scanning speed of 2°/minute, having a step of 0.05°. The XRD spectrum analysis was performed using the PDXL 2 program, and the crystalline compounds were identified using the ICDD database (PDF 5+ 2024). Fig. 7 shows diffractogram obtained by XRD for the $Zr_{75}Er_{25}$ sample.

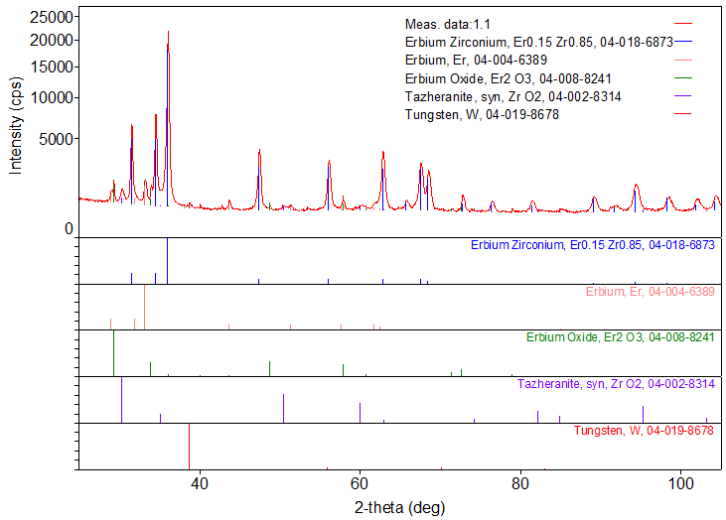

Fig. 7. XRD Diffractogram of $Zr_{75}Er_{25}$

From Fig. 7, it can be observed that the XRD analysis of the $Zr_{75}Er_{25}$ sample reveals the presence of several crystalline phases. These include an Er–Zr phase with nominal composition $Er_{0.15}Zr_{0.85}$, corresponding to the blue diffraction peaks, metallic erbium associated with the yellow peaks, erbium oxide (Er_2O_3) identified by the green peaks, zirconium oxide (ZrO_2) corresponding to the purple peaks, and tungsten, indicated by the red peaks.

The presence of the $Er_{0.15}Zr_{0.85}$ phase can be attributed to the diffusion of erbium atoms into the zirconium lattice during the heat treatment, leading to the formation of a Zr-rich solid solution with partial substitution of zirconium sites by erbium atoms. The resulting phase reflects the local atomic distribution within the alloy, with approximately 15 at.% erbium incorporated into the zirconium-based crystal structure.

The detection of erbium and zirconium oxides is associated with partial oxidation of the sample during processing or exposure to the atmosphere, both elements exhibiting a high affinity for oxygen. The presence of tungsten is attributed to residual impurities originating from the initial erbium raw material. In

the sample, the metallic erbium is found due to the atoms of it that did not react with zirconium.

The semi-quantitative analysis of the phases found in $Zr_{75}Er_{25}$ sample is presented in Table 7. The determination of the concentrations of the compounds in the sample was performed by the Whole Powder Pattern Fitting (WPPF) method, which allows simultaneous refinement of diffraction intensity and diffracted angle under pattern-fitting conditions [25].

Table 7

Semi-quantitative phase analysis of $Zr_{75}Er_{25}$

No.	Phase	Chemical formula	ICDD (PDF 5+ 2024) DB	Content (%)	Calculated density (g/cm^3)
1	Erbium Zirconium	$Er_{0.15}Zr_{0.85}$	04-018-6873	88.9	7.047
2	Erbium	Er	04-004-6389	5.0	9.042
3	Erbium oxide	Er_2O_3	04-008-8241	2.44	8.623
4	Zirconium oxide	ZrO_2	04-002-8314	3.5	6.146
5	Tungsten	W	04-019-8678	0.22	17.214

Quantitative phase analysis of the Zr_{75}-Er_{25} sample, reveals a high fraction of a Zr-rich solid solution, under the form of $Er_{0.15}Zr_{0.85}$, an alloy formed following sintering, and also the presence of a low concentration of oxides and impurities (below 5%).

The X-ray diffractogram of $Zr_{50}Er_{50}$ sample was obtained using CuKα radiation in the 2θ measurement range: (25°-105°), by continuous scanning, with a scanning speed of 2°/minute, having a step of 0.05°. The XRD spectrum analysis was performed using the PDXL 2 program, and the crystalline compounds were identified using the ICDD database (PDF 5+ 2024). Fig. 8 shows the diffractogram for the $Zr_{50}Er_{50}$ sample.

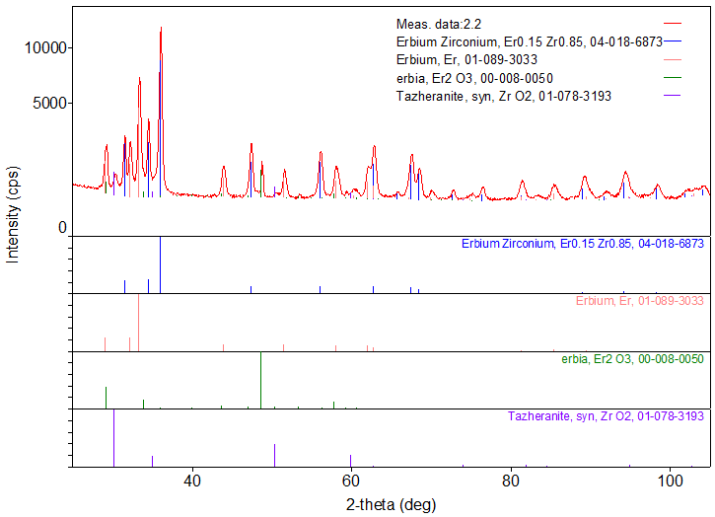

Fig. 8. XRD Diffractogram of $Zr_{50}Er_{50}$

From Fig. 8 it can be seen that, following the XRD analysis of $Zr_{50}Er_{50}$ sample, were identified these phases: erbium-zirconium intermetallic alloy ($Er_{0.15}Zr_{0.85}$), associated with the blue peak, erbium (Er), associated with the orange spectrum, erbium oxide (Er_2O_3), identified by the green spectrum and zirconium oxide (ZrO_2), associated with the purple spectrum. The presence of the $Er_{0.15}Zr_{0.85}$ phase is justified by the diffusion of erbium atoms into zirconium locally, forming a Zr-rich solid solution. Erbium and zirconium oxides in the sample appeared because of the interaction between the sample with the atmosphere. Also, a quantity of pure metallic erbium is present because a mass of erbium did not interact with zirconium during the sintering treatment.

The semi-quantitative analysis of the phases found in $Zr_{50}Er_{50}$ sample is presented in Table 8.

Table 8

Semi-quantitative phase analysis of $Zr_{50}Er_{50}$

No.	Phase	Chemical formula	ICDD (PDF 5+ 2024) DB	Content (%)	Calculated density (g/cm^3)
1	Erbium Zirconium	$Er_{0.15}Zr_{0.85}$	04-018-6873	59.1	7.035
2	Erbium	Er	01-089-3033	26.6	9.156
3	Erbium oxide	Er_2O_3	00-008-0050	6.9	8.596
4	Zirconium oxide	ZrO_2	01-078-3193	7.4	6.084

From the results, it can be seen a presence of 59.1% of the Zr-rich solid solution, a low presence of erbium and zirconium oxides, but also a relatively high content of pure metallic erbium (26.6%), which is explained by the isolation of erbium grains and their lack of interaction with zirconium.

6. Conclusions

Following the experimental work carried out in this paper, two sintered compacts were obtained, having the following compositions: $Zr_{75}Er_{25}$ and $Zr_{50}Er_{50}$.

The precursors were obtained by hydriding the raw materials, at temperature 750 ^oC, in H_2, obtaining ZrH_2 and ErH_3. The hydrides obtained were characterized and presence of hydrides of zirconium and erbium was confirmed. The presence of zirconium and erbium oxides was observed, in small quantities, this being due to the interaction of the powders with atmosphere. The hydrides obtained were mechanically processed, mixed and pressed.

After sintering, the samples were characterized using multiple analytical techniques. The results indicate that the Zr_xEr_{1-x} compacts with x = 0.50 and 0.75 exhibit relative densities exceeding 90% of their theoretical values, demonstrating effective densification during the sintering process.

SEM–EDS analyses reveal that, during heat treatment, erbium undergoes enhanced atomic mobility and diffuses into the zirconium matrix, leading to the formation of a multiphase microstructure consisting of Zr-rich solid solution phase.

Furthermore, quantitative elemental analysis of oxygen shows a higher oxygen concentration in erbium-rich regions, confirming the stronger affinity of erbium for oxygen and its increased tendency to form oxide phases compared to zirconium.

XRD analysis indicates that the samples are composed of several crystalline phases, namely an Er–Zr phase with nominal composition $Er_{0.15}Zr_{0.85,}$ metallic erbium (Er), erbium oxide (Er_2O_3), zirconium oxide (ZrO_2), and tungsten. The objective of sintering the Zr_xEr_{1-x} compacts (x = 0.50 and 0.75) is to obtain materials with a high degree of homogeneity, enhanced densification, and the maximum possible fraction of the Er–Zr alloyed phase. Based on the phase analysis, the $Zr_{75}Er_{25}$ sample exhibits the highest content of the Er–Zr phase, accounting for approximately 88.9 wt.% of the alloyed Er–Zr phase.

Future investigations will focus on evaluating the hydrogen absorption and desorption behavior of these materials, including storage capacity, kinetics, thermodynamic stability, and cyclic durability under repeated hydrogenation–dehydrogenation cycles. Additionally, optimization of sintering parameters and compositional tuning within the Zr–Er system may further enhance phase purity and hydrogen diffusion pathways. Such studies are expected to clarify the structure–property–performance relationships governing hydrogen storage in Zr–Er-based materials and to support their potential integration into advanced hydrogen energy systems. Zr–Er alloys obtained via powder metallurgy are promising hydrogen storage materials due to their ability to form stable hydrides, their microstructure with high surface area and controlled porosity. The combination of Zr and Er provides multiple sites for hydrogen uptake, while powder metallurgy processing ensures fast diffusion and hydriding/dehydriding cycles.

R E F E R E N C E S

[1] Bartosz Ceran, Agata Mielcarek, Qusay Hassan, Janusz Teneta and Marek Jaszczur, "Aging effects on modelling and operation of a photovoltaic system with hydrogen storage," *Applied Energy,* vol. 297, September 2021.

[2] Sammer Algburi, Hassan Munther, Omer Al-Dulaimi, Hassan Falah Fakhruldeen, I.B. Sapaev, Karrar Fadhil Khalaf Al Seedi, Doaa H. Khalaf, Feryal Ibrahim Jabbar, Qusay Hassan, Ali Khudhair and Grace Nakimera, "Green Hydrogen Role in Sustainable Energy Transformations: A Review," *Results in Engineering,* vol. 26, 2025.

[3] Angel Berenguer-Murcia, Juan Pablo Marco-Lozar and Diego Cazorla-Amoros, "Hydrogen Storage in Porous Materials: Status, Milestones, and Challenges," *The Chemical Record,* vol. 18, no. 7-8, pp. 900-912, 2018.

[4] Mrinmoy Kumar Sarmah, Tej Pratap Singh, Pankaj Kalita and Anupam Dewan, "Sustainable hydrogen generation and storage – a review," *Royal Society of Chemistry,* vol. 13, no. 36, pp. 25253-25275, 2023.

[5] Abdalla M. Abdalla, Shahzad Hossain, Ozzan B. Nisfindy, Atia T. Azad, Mohamed Dawood and Abul K. Azad, "Hydrogen production, storage, transportation and key challenges with applications: A review," *Energy Conversion and Management,* vol. 165, pp. 602-627, 2018.

[6] Joakim Andersson and Stefan Gronkvist, "Large-scale storage of hydrogen," *International Journal of Hydrogen Energy,* vol. 44, no. 23, pp. 11901-11919, 2019.

[7] Muhammad R. Usman, "Hydrogen storage methods: Review and current status," *Renewable and Sustainable Energy Reviews,* vol. 167, p. 112743, 2022.

[8] Emmanuel I. Epelle, Kwaghtaver S. Desongu, Winifred Obande, Adekunle A. Adeleke, Peter P. Ikubanni, Jude A. Okolie and Burcu Gunes, "A comprehensive review of hydrogen production and storage: A focus on the role of nanomaterials," *International Journal of Hydrogen Energy,* vol. 47, no. 47, pp. 20398-20431, 2022.

[9] Nejc Klopcic, Ilena Grimmer, Franz Winkler, Markus Sartory and Alexander Trattner, "A review on metal hydride materials for hydrogen storage," *Journal of Energy Storage,* Vols. 72, Part B, p. 108456, 2023.

[10] Marolop Simanullang and Laurent Prost, "Nanomaterials for on-board solid-state hydrogen storage applications," *International Journal of Hydrogen Energy,* vol. 47, no. 69, pp. 29808-29846, 2022.

[11] Eberle U., Felderhoff M. and Schuth F., "Chemical and physiscal solutions for hydrogen storage," *Angew Chem Int Ed Engl.,* vol. 48, no. 36, 2009.

[12] R. Kirchheim and A. Pundt, "Hydrogen in Metals," in *Physical Metallurgy (Fifth Edition)`*, 2014, pp. 2597-2705.

[13] E. Zuzek, J. Abriata and A. San-Martin, "The H-Zr (Hydrogen-Zirconium System)," *Bulletin of Alloy Phase Diagrams,* vol. 11, pp. 385-395, 1990.

[14] C. Armantrout, "Quarterly Metallurgical Progress Report No. 3," 1959.

[15] B. Love, "Wright Air Development Division Technical Report 60-74. The metallurgy of Yttrium and the rare earth metals. Part I. Phase relationships," Hannover, 1960.

[16] M. Copeland and H. Kato, "Rare-earth-rich alloys," in *Proc. of the Symposium on Physics and Material Problems of Reactor Control Rods*, Vienna, 1963.

[17] G. Narayanan and R. Wang, "An electron microscopy study of the metastable structures in splat-cooled erbium-zirconium alloys," *Journal of Materials Science,* vol. 11, pp. 1667-1679, 1976.

[18] J. Jourdan, C. Toffolon and J.-M. Joubert, "Experimental re-determination and thermodynamic assessment of the erbium-zirconium system," *Journal of Nuclear Materials,* vol. 402, pp. 102-107, 2010.

[19] William D. Callister Jr. and David G. Rethwisch, Materials Science and Engineering. An Introduction; Tenth Edition, WILEY, 2018.

[20] Randall M. German, Powder Metallurgy and Particulate Materials Processing: The Processes, Materials, Products, Properties and Applications, Metal Powder Industries Federation, 2005.

[21] Reza Abbaschian and Robert E. Reed-Hill, Physical Metallurgy Principles, Cengage Learning, 2008.

[22] C. Suryanarayana, "Mechanical alloying and milling," *Progress in Materials Science,* vol. 46, no. 1-2, pp. 1-184, January 2001.

[23] Enghag P., Encyclopedia of the Elements. Technical Data. History. Processing and Applications, Wiley-VCH Verlag, 2004.

[24] Baciu Constantin, Ioan Alexandru, Radu Popovici and Maria Baciu, Știința Materialelor Metalice, București: Editura Didactică și Pedagogică, 1996.

[25] Md. Ashraful Alam, Shanawaz Ahmed, Raton Kumar Bishwas, Sabrina Mostofa and Shirin Akter Jahan, "X-ray crystallographic diffraction study by whole powder pattern fitting (WPPF) method: Refinement of crystalline nanostructure polymorphs TiO2," *South African Journal of Chemical Engineering,* vol. 51, pp. 68-77, 2025.